

# Towards dynamic metabolic network measurements by multi-dimensional NMR-based fluxomics

Yasuyo Sekiyama<sup>a</sup>, Jun Kikuchi<sup>a,b,c,\*</sup>

<sup>a</sup> RIKEN Plant Science Center, 1-7-22 Suehiro-cho, Tsurumi-ku, Yokohama-shi 235-0045, Japan

<sup>b</sup> CREST, Japan Science and Technology Agency, 4-1-8 Hon-cho, Kawaguchi-shi 332-0012, Japan

<sup>c</sup> Graduate School of Bioagricultural Sciences, Nagoya University, 1 Furo-cho, Chikusa-ku, Nagoya-shi 464-8601, Japan

Received 19 January 2007; received in revised form 30 March 2007

Available online 25 May 2007

## Abstract

Novel technologies for measuring biological systems and methods for visualizing data have led to a revolution in the life sciences. Nuclear magnetic resonance (NMR) techniques can provide information on metabolite structure and metabolic dynamics at the atomic level. We have been developing a new method for measuring the dynamic metabolic network of crude extracts that combines [<sup>13</sup>C]<sub>6</sub>glucose stable isotope labeling of *Arabidopsis thaliana* and multi-dimensional heteronuclear NMR analysis, whereas most conventional metabolic flux analyses examine proteinogenic amino acids that are specifically labeled with partially labeled substrates such as [2-<sup>13</sup>C]<sub>1</sub>glucose or 10% [<sup>13</sup>C]<sub>6</sub>glucose. To show the validity of our method, we investigated how to obtain information about biochemical reactions, C–C bond formation, and the cleavage of the main metabolites, such as free amino acids, in crude extracts based on the analysis of the <sup>13</sup>C–<sup>13</sup>C coupling pattern in 2D-NMR spectra. For example, the combination of different extraction solvents allows one to distinguish complicated <sup>13</sup>C–<sup>13</sup>C fine couplings at the C2 position of amino acids. As another approach, f1–f3 projection of the HCACO spectrum also helps in the analysis of <sup>13</sup>C–<sup>13</sup>C connectivities. Using these new methods, we present an example that involves monitoring the incorporation profile of [<sup>13</sup>C]<sub>6</sub>glucose into *A. thaliana* and its metabolic dynamics, which change in a time-dependent manner with atmospheric <sup>12</sup>CO<sub>2</sub> assimilation.

© 2007 Elsevier Ltd. All rights reserved.

**Keywords:** Metabolic network; Stable isotope labeling; Heteronuclear multi-dimensional NMR; <sup>13</sup>C–<sup>13</sup>C fine coupling; Crude extract; Extraction solvents

## 1. Introduction

Nuclear magnetic resonance (NMR) spectroscopy is one of the most powerful and widely used techniques for determining structure and analyzing the environment and physical properties of molecules. NMR methods are relatively insensitive, and only signals from compounds present in relatively large amounts (at least nmol quantities) can be detected in spectra (Korir et al., 2005; Li et al., 2006). As metabolic engineering usually results in the accumulation

of relatively high concentrations of metabolites, this insensitivity is often less restrictive for compound detection and identification than for other areas of biochemistry. NMR signals can be detected from the nuclei of many isotopes; <sup>1</sup>H, <sup>13</sup>C, <sup>15</sup>N, and <sup>31</sup>P are the most widely used for biological NMR spectroscopy (Ratcliffe et al., 2001; Ratcliffe and Shachar-Hill, 2001, 2005). The relevant magnetic isotope of carbon is <sup>13</sup>C; its low natural abundance of only 1.11% contributes to the considerably lower sensitivity of <sup>13</sup>C NMR compared with <sup>1</sup>H NMR. Accordingly, the application of <sup>13</sup>C NMR in unlabeled systems is largely confined to the detection of the most abundant metabolites (Ratcliffe and Shachar-Hill, 2001). Stable isotope labeling is used to enhance the signal intensities of relatively low-sensitivity nuclei such as <sup>13</sup>C (Ratcliffe and Shachar-Hill, 2001).

\* Corresponding author. Address: RIKEN Plant Science Center, 1-7-22 Suehiro-cho, Tsurumi-ku, Yokohama-shi 235-0045, Japan. Tel.: +81 45 503 9490; fax: +81 45 503 9489.

E-mail address: [kikuchi@psc.riken.jp](mailto:kikuchi@psc.riken.jp) (J. Kikuchi).

Labeling with  $^{13}\text{C}$  can also be used to monitor the changes in carbon–carbon connectivity in metabolic processes, using bondomer analysis. Bondomers, which possess  $^{13}\text{C}$ – $^{13}\text{C}$  bonds at specific places within a molecule, can be distinguished by analyzing the characteristic splitting of the signals in NMR spectra (London, 1988; Ratcliffe and Shachar-Hill, 2006). In particular, one-bond  $^{13}\text{C}$ – $^{13}\text{C}$  couplings ( $^1J_{\text{CC}}$ ) undergo marked variation on substitution and in the electronic structure of their carbon–carbon bonds (Mooney and Winson, 1969; Maciel, 1974; Hansen, 1978; Krivin and Kalabin, 1988; Buncel and Jones, 1991; Kamińska-Trela, 1995, and references cited therein), facilitating unambiguous identification and quantification of each bondomer.

As a technique for analyzing metabolic flux, one-dimensional (1D)  $^{13}\text{C}$  NMR analysis of proteinogenic amino acids (and roughly purified primary metabolites) with partially stable isotope-labeled substrates such as  $[2\text{-}^{13}\text{C}_1]\text{glucose}$  or 10%  $[^{13}\text{C}_6]\text{glucose}$  is well established (de Graaf et al., 2000; Petersen et al., 2000; Roberts, 2000; Roscher et al., 2000; Glawischnig et al., 2001; Jones et al., 2001; Kruger et al., 2003). Compared with feeding experiments using a specifically labeled substrate, uniform isotope labeling of plants increases detectable metabolites, potentially making it possible to elucidate more complicated metabolic networks. In recent years, we have reported methods for stable isotope labeling in higher plants using carbon or nitrogen, two of the largest components of organic compounds (Kikuchi et al., 2004; Kikuchi and Hirayama, 2006, 2007). For example, the uptake of  $[^{13}\text{C}_6]\text{glucose}$  via the roots or the assimilation of  $^{13}\text{CO}_2$  into higher plants results in the incorporation of the  $^{13}\text{C}$  nucleus instead of  $^{12}\text{C}$  in hundreds of organic compounds. However, the 1D-NMR technique is not applicable when attempting to follow bondomers in hundreds of uniformly  $^{13}\text{C}$ -labeled metabolites. By contrast, 2D NMR techniques allow the resolution of overlapping signals in the second dimension (Szyperski, 1995; Schmidt et al., 1999; van Winden et al., 2002; Yang et al., 2002) and can be used not only for spectral dispersion but also for assigning various molecules in complex systems (Govil, 2004). Furthermore, indirect detection techniques such as 2D  $^{13}\text{C}$ -heteronuclear single quantum coherence (HSQC) pulse sequences increase the sensitivity of the experiments (Bodenhausen and Ruben, 1980). Therefore, a combination of uniform stable isotope labeling with 2D heteronuclear NMR allows the resolution of hundreds of  $^{13}\text{C}$ – $^{13}\text{C}$  bondomers in  $^{13}\text{C}$ -labeled plant extracts. Combining fractional labeling, for example, 10%  $[\text{U-}^{13}\text{C}]\text{sucrose}$  and 90% naturally abundant sucrose, allowed the analysis of the  $^{13}\text{C}$ – $^{13}\text{C}$  coupling pattern of the signals in 2D  $^1\text{H}$ – $^{13}\text{C}$  spectra of protein or starch hydrolysate using refined deconvolution software (Szyperski, 1995; Szyperski et al., 1996; Siram et al., 2004). However, the analysis of  $^{13}\text{C}$ – $^{13}\text{C}$  coupling patterns remains complicated in experimental measurements of crude extracts from organisms because they contain all soluble metabolites—not only free amino acids and carbohydrates but also organic acids, lipid compounds,

etc.—and result in the coexistence of multiple bondomers and overlapping split signals. Signal overlap is caused mainly by the close chemical shifts of signals or close  $^1J_{\text{CC}}$  values. In some cases, these may be resolved by increasing the amount of acquired data, however, this is limited by the line width, and more importantly, it is necessary to reduce the total acquisition time for metabolome usage.

Recently, several reports have shown that metabolic flux analysis can be extended not only to conventional targeted analysis but also to comprehensive analysis, known as fluxome or fluxomics (Sauer et al., 1999; Nielsen, 2003; Kromer et al., 2004; Sauer, 2004; Birkemeyer et al., 2005; Zamboni and Sauer, 2005; Sauer, 2006; Tang et al., 2007). This concept might contribute significantly to promoting systems biology in the era of post-metabolomics (Sanford et al., 2001; Lee et al., 2005; Nielsen and Oliver, 2005; Wang et al., 2006; Wendish et al., 2006), although the current technology might still be insufficient. Even metabolome analysis is limited by chemical complexity, metabolic heterogeneity, dynamic range, and ease of extraction. In particular, a major drawback may be measurement technology (Hall, 2005). Among the many available analytical platforms are GC/MS, LC/MS, CE/MS, FT/MS, and NMR, but these have several limitations (Pan and Raftery, 2007). Therefore, we have focused on developing new methods for metabolome and fluxome analysis. The measurement technologies discussed here constitute our first report on NMR-based fluxomics.

Our strategies differ from NMR-based targeted flux analysis in that we (1) start with uniform labeling with  $^{13}\text{C}$ , (2) use crude plant extracts instead of proteinogenic amino acids, and (3) analyze the time-dependent changes of the bondomer composition at each growth stage in order to follow dynamic metabolic networks. To obtain detailed information on metabolites at the atomic level, the analysis time is inevitably lengthened by a purification step, with the consequent loss of valuable information on the removed metabolites. In addition, there is a long acquisition time owing to lower labeling ratios and larger data points. Here, we show how to distinguish the complicated  $^{13}\text{C}$ – $^{13}\text{C}$  bondomers in 2D-NMR spectra by using different extraction solvents to change the  $^1J_{\text{CC}}$  values and different NMR pulse sequences to detect the  $^{13}\text{C}$ – $^{13}\text{C}$  connectivities from a different direction. Using these methods, we present an example of bondomer analysis combined with uniform stable isotope labeling used to measure a metabolic network.

## 2. Results and discussion

### 2.1. Measuring $^{13}\text{C}$ – $^{13}\text{C}$ fine couplings using 2D-NMR

#### 2.1.1. Combining different extraction solvents for 2D $^1\text{H}$ – $^{13}\text{C}$ HSQC analysis

Several factors contribute to the variation in  $^1J_{\text{CC}}$ : the coupling mechanism itself, the electronic influence of substituents, the orientation of bonds and steric effects, the

effects of unshared electron pairs, and the effects of solvents. It has been suggested that  $^1J_{CC}$  is less sensitive to temperature and sample concentration (Krivin and Kalabin, 1988). The effects of the solvent are manifested in the variation in  $^1J_{CC}$ . Magnetic shielding is induced by the magnetic moments of neighboring molecules and intermolecular electrostatic interactions. We compared the  $^{13}\text{C}$ – $^{13}\text{C}$  coupling pattern and  $^{13}\text{C}$ – $^{13}\text{C}$  connectivities that could be distinguished in the main metabolites in *Arabidopsis thaliana* using two extraction solvents: deuterated methanol (MeOD)/4-(2-hydroxyethyl)-1-piperazine ethanesulphonic acid (HEPES) and hexafluoroacetone trideuterate (HFA)/HEPES. Fig. 1 shows a scheme for analyzing the  $^{13}\text{C}$ – $^{13}\text{C}$  coupling pattern in 2D  $^1\text{H}$ – $^{13}\text{C}$  HSQC spectra. First, *A. thaliana* was uniformly labeled by the root uptake of  $^{13}\text{C}_6$ glucose. It should be noted that we needed only 3 mg of dry plant material for an experiment, which was performed by the high-sensitive  $^1\text{H}$  detection technique using cryogenically cooled probe. The use of cryogenic probe has become widespread. It enhances sensitivity espe-

cially in non-polar organic solvents due to low dielectric property (Horiuchi et al., 2005), and enables us to use low-concentration samples. We note that reproducibility of our NMR methods is extremely high due to high stability of NMR experiments. Furthermore, sampling of several plants can help to avoid experimental errors of NMR results due to individual metabolic differences. Our established  $^{13}\text{C}$  labeling, sampling and 2D  $^1\text{H}$ – $^{13}\text{C}$  HSQC analysis exhibited high reproducibility as described in essentially same experiments reported in Tian et al. (2007).

During atmospheric  $^{12}\text{CO}_2$  assimilation,  $^{13}\text{C}$ – $^{13}\text{C}$  bonds originating from  $^{13}\text{C}_6$ glucose were cleaved, and the uniformly labeled metabolites became a set of multiple bondomers that depended on the biosynthetic pathways involved. Fig. 1a and b show the  $^1\text{H}$ – $^{13}\text{C}$  HSQC spectra of the MeOD/HEPES extract of  $^{13}\text{C}_6$ glucose-labeled *A. thaliana* sampled at day 13 and an expanded view of the asparagine region, respectively. The signals were assigned by comparing the chemical shifts with the standard compound database and 3D HCCH-COSY analysis (Kay

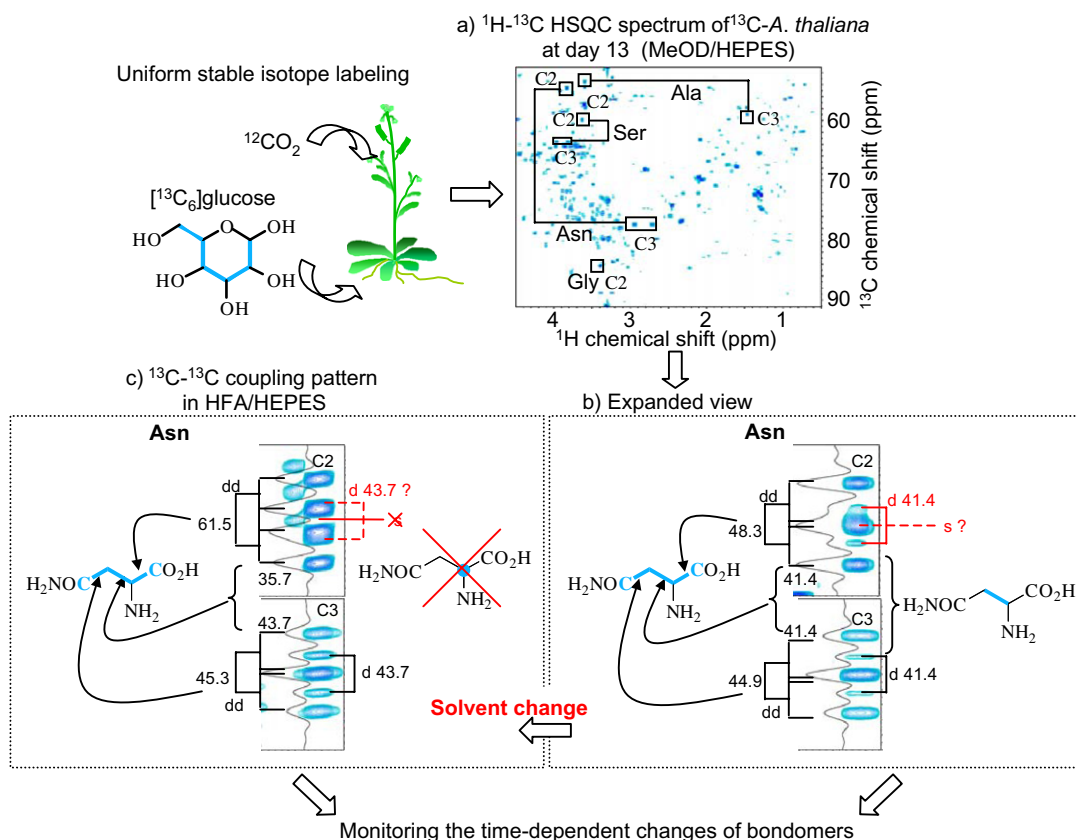


Fig. 1. Scheme for analyzing the  $^{13}\text{C}$ – $^{13}\text{C}$  coupling patterns in 2D  $^1\text{H}$ – $^{13}\text{C}$  HSQC spectra and examples of the effects of solvents and deduced bondomers. The carbon atoms of amino acids are successively numbered from carboxyl carbon (C1) next to the carbon atoms carrying amino group. Coupling constants are shown alongside in Hz. The multiplet peaks are: s, singlet; d: doublet; dd: double doublet. Blue bonds indicate deducible  $^{13}\text{C}$ – $^{13}\text{C}$  connectivities. Details of all the measured coupling constants and the amount of each bondomer are listed in Table 1. (a) Aliphatic region of  $^{13}\text{C}_6$ glucose-labeled *A. thaliana* sampled at day 13 (MeOD/HEPES). The amino acid signals discussed in this paper are indicated. The spectral window and offset frequency in the f1 dimension were 7042.593 Hz (40 ppm) and 11971.59 Hz (68 ppm), respectively. The spectral window and offset frequency in the f2 dimension were 11160.7 Hz (16 ppm) and 2333.70 Hz (3.3 ppm), respectively. (b) Expanded view of the C–2 and C–3 regions of asparagine.  $^1J_{\text{C1-C2}} = 48.3$  Hz,  $^1J_{\text{C2-C3}} = 41.4$  Hz, and  $^1J_{\text{C3-C4}} = 44.9$  Hz. (c) Expanded view of the C–2 and C–3 regions of asparagine in the  $^1\text{H}$ – $^{13}\text{C}$  HSQC spectrum of  $^{13}\text{C}_6$ glucose-labeled *A. thaliana* sampled at day 13 (HFA/HEPES).  $^1J_{\text{C1-C2}} = 61.5$  Hz,  $^1J_{\text{C2-C3}} = 43.7$  Hz, and  $^1J_{\text{C3-C4}} = 45.3$  Hz. The  $^1J_{\text{C2-C3}}$  value observed at C2 looks smaller (35.7 Hz) due to the overlapped doublet signal arising from the  $[2,3-^{13}\text{C}_2]$  bondomer.

et al., 1990a). The carbon atoms of amino acids are successively numbered from carboxyl carbon (C1) next to the carbon carrying amino group. Although it should be possible to estimate the bondomer composition from the integrated information on the coupling pattern, intensity, and line width of the signals of all the carbons in any given molecule, we focused on the coupling pattern at the C2 position and the  $^{13}\text{C}$ – $^{13}\text{C}$  connectivities that could be deduced from this in order to simplify the explanation. The expanded view of the C2 signal of asparagine in MeOD/HEPES (Fig. 1b) shows a larger double doublet peak (*dd*) and a smaller doublet peak (*d*), indicating C1–C2–C3 and C2–C3 connectivities, respectively. In this case, the  $^1J_{\text{CC}}$  value of C1–C2 is extremely close to that of C2–C3, and the central two peaks of the *dd* are fused in the digital resolution (f1 spectral window of 7042.593 Hz and 700 f1 data points, zero filled to 4096), such that any overlapped singlet peak(s) cannot be distinguished. Given the difficulty in estimating the composition of bondomers from the intensity or line width of overlapped multiplet signals, we examined different extraction solvents. Asparagine signals of the HFA/HEPES extract of the same  $^{13}\text{C}$ -*A. thaliana* sample are shown in Fig. 1c. In this solvent, the difference between the  $^1J_{\text{CC}}$  values of C1–C2 and C2–C3 is sufficient to resolve the two central peaks of *dd* and to distinguish these from the singlet peak. At day 13, no singlet peak was observed at the C2 of asparagine, so  $[2\text{-}^{13}\text{C}_1]$ - and  $[2,4\text{-}^{13}\text{C}_2]$ -bondomers were clearly excluded from the theoretically possible bondomer complement. Although the doublet peak indicating C2–C3 connectivity is hindered by C2 *dd* peaks in HFA/HEPES, it can be clearly distinguished in MeOD/HEPES, as described above. The  $^{13}\text{C}$ – $^{13}\text{C}$  bond connectivities deduced from the C2 coupling pattern are indicated by blue lines in Fig. 1b and c and were supported by the coupling pattern of C3. Details of all the measured coupling constants are listed in Table 1. To verify the advantages of bondomer analysis in different solvents, we should give other examples of solvent effects on  $^1J_{\text{CC}}$ . We examined variation in the  $^1J_{\text{CC}}$  values not only in MeOD/HEPES, HFA/HEPES but also potassium phosphate (KPi) buffer and dimethyl sulfoxide (DMSO)- $d_6$  using a  $^{13}\text{C}$ -labeled mixture of standard compounds (supplementary section). There are remarkable changes in coupling constants by changing solvents at the carbon substituted with electrically charged functional group, such as C2 of amino acids, C2 of organic acids, while little variations were observed in the coupling constants of the carbon possessing uncharged functional group, such as alkyl group of leucine, C1 of glucose. They are apparently due to strong electric field effects arising from charged functional groups. Additional advantage of the measurement using different solvents is that it separates overlapped signals via chemical shift changes. For instance, overlapped signals observed in DMSO- $d_6$ , such as leucine C4, proline C2 and C4 and succinate C2, are separated in MeOD/HEPES and HFA/HEPES. These data also support the advantages of bondomer analysis in different solvents.

As described above, overlapped multiplet can be separated using different extraction solvents. It gives more detailed information on metabolic network at the atomic level using highly sensitive 2D  $^1\text{H}$ – $^{13}\text{C}$  HSQC analyses. However, we have to consider undetectable bondomers with this pulse sequence. To analyze complex networks between multiple metabolic pathways, bondomers of measurable metabolites have to be completely analyzed. In this context, we decided to examine combination of 2D  $^1\text{H}$ – $^{13}\text{C}$  HSQC experiment and other heteronuclear NMR techniques.

### 2.1.2. 2D HCACO analysis

2D  $^1\text{H}$ – $^{13}\text{C}$  HSQC analyses with different extraction solvents detect only the carbons bonded directly to hydrogen. In our strategy, almost all of the carbons of the metabolites were labeled, including quaternary and carbonyl carbons. Therefore, we can take advantage of several pulse sequences involving  $^{13}\text{C}$ – $^{13}\text{C}$  magnetization transfer via  $^1J_{\text{CC}}$  couplings, such as carbon–carbon–proton and proton–carbon–carbon–proton techniques. Carbonyl carbon is one of the most important functional groups, and most primary metabolites possess carbonyl groups. In addition, carbonyl carbon is susceptible to nucleophilic attack by biological nucleophiles to form C–C bonds. In this context, we performed HCACO experiments (Kay et al., 1990a; Grzesiek and Bax, 1993), which correlate  $\text{H}\alpha$  and  $\text{C}\alpha$  (C2) shifts to intramolecular carbonyl (C1) shifts. To determine the exact  $^1J_{\text{C1-C2}}$  values, we performed  $\text{C}\alpha$ -coupled type HCACO experiments that show approximately 55 Hz  $^{13}\text{C}$ – $^{13}\text{C}$  doublet couplings in the f1 (C1) dimension. As an example, Fig. 2 shows the f1–f3 projection of the  $\text{C}\alpha$ -coupled HCACO spectrum of  $[^{13}\text{C}_6]$ glucose-labeled *A. thaliana* sampled at day 13. In this spectrum, all of the carbonyl carbons of glycine, serine, and asparagine exhibit a clear doublet showing exact  $^1J_{\text{C1-C2}}$  values. This analysis affords accurate  $^1J_{\text{C1-C2}}$  values of carbonyl compounds and is especially useful with metabolites for which the  $^1J_{\text{CC}}$  values of C1–C2 are difficult to determine from  $^1\text{H}$ – $^{13}\text{C}$  HSQC analysis, as with asparagine or serine in MeOD/HEPES (the coupling pattern and coupling constant of C2 in serine are shown in Fig. 5). In addition to combining different

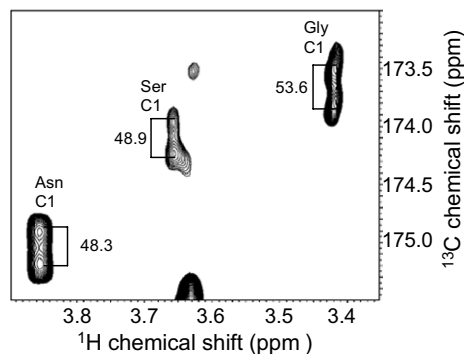


Fig. 2. Expanded view of the f1–f3 projection of the  $\text{C}\alpha$ -coupled HCACO spectra of  $[^{13}\text{C}_6]$ glucose-labeled *A. thaliana* sampled at day 13 (MeOD/HEPES). Each  $^1J_{\text{C1-C2}}$  value is shown alongside in Hz.



extraction solvents, this method provides another way of determining accurate  $^1J_{\text{C1-C2}}$  values and is useful for estimating bondomer composition.

Concerning measuring dynamic metabolic networks, the f1–f3 projection of the highly sensitive C $\alpha$ -decoupled (normal) HCACO experiment gives information about the amount of bondomers possessing C1–C2  $^{13}\text{C}$ – $^{13}\text{C}$  bonds. For example, Fig. 3 compares the signal intensity ratio of C1 in the amino acids of [ $^{13}\text{C}_6$ ]glucose-labeled *A. thaliana* sampled at days 13 and 10. Increased signal intensity, as seen with serine, glycine, and proline, suggests the accumulation of bondomers possessing C1–C2  $^{13}\text{C}$ – $^{13}\text{C}$  connectivity. This may have resulted from enhanced biosynthesis of the metabolite from precursors that possess a  $^{13}\text{C}$ – $^{13}\text{C}$  bond at the corresponding position, or  $^{13}\text{C}$ – $^{13}\text{C}$  bond formation at C1–C2 via the C–C coupling reaction. Conversely, decreased signal intensity, as seen with alanine and asparagine, suggests a reduction of bondomers possessing C1–C2  $^{13}\text{C}$ – $^{13}\text{C}$  connectivity, which may have occurred because the  $^{13}\text{C}$  labeling of biosynthetic precursors was diluted at the corresponding position by the assimilation of atmospheric  $^{12}\text{CO}_2$  or because the C–C coupling reaction occurred between  $^{13}\text{C}$  and  $^{12}\text{C}$  precursors. Additional information about the other carbons of biosynthetic precursors and products of catabolic processes is required to explain these results. Here, we have indicated that detailed example for the metabolic flux information of five amino acids can be measured by following of  $^1J_{\text{CC}}$  and relative signal intensities in the HCACO. In the next stage, from overall time-dependent changes of [ $^{13}\text{C}_6$ ]glucose incorporation for all measurable metabolites to the detailed metabolic flux analysis should be needed in order to discuss dynamic network measurements in *A. thaliana*.

## 2.2. Example of the time-dependent changes in $^{13}\text{C}$ – $^{13}\text{C}$ coupling patterns with $^{12}\text{CO}_2$ assimilation in *A. thaliana*

### 2.2.1. Overall changes in $^{13}\text{C}$ labeling during the growth of *A. thaliana*

Two strategies for analyzing  $^{13}\text{C}$ – $^{13}\text{C}$  coupling patterns and deducible bondomers were demonstrated, as described above. By combining these strategies with uniform stable isotope labeling of plants, we are developing a method for measuring dynamic metabolic networks. In contrast to conventional metabolic flux analysis, which involves specific labeling using partially labeled substrates, we examined uniform  $^{13}\text{C}$  labeling by [ $^{13}\text{C}_6$ ]glucose to increase detectable metabolites and to take advantage simultaneously of several NMR pulse sequences. We expected to observe time-dependent changes in the bondomer composition during growth because plants assimilate atmospheric  $^{12}\text{CO}_2$ . Overall changes in  $^{13}\text{C}$  labeling in time-dependent manner should indicate above information. Therefore, the time course of [ $^{13}\text{C}_6$ ]glucose and  $^{13}\text{CO}_2$  incorporation into *A. thaliana* was monitored using the ratio of the total signal intensity and the number of all signals observed in the  $^1\text{H}$ – $^{13}\text{C}$  HSQC spectra (Fig. 4). Plants were harvested

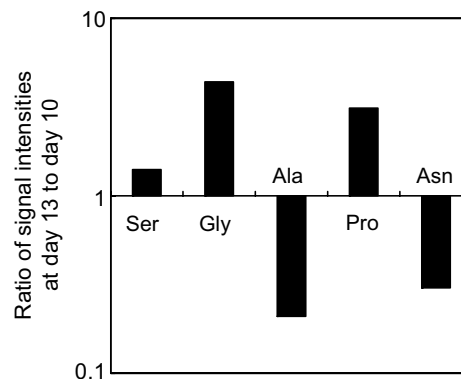


Fig. 3. Signal intensity ratio of the C1 carbonyl carbon of amino acids observed in C $\alpha$ -decoupled HCACO spectra of [ $^{13}\text{C}_6$ ]glucose-labeled *A. thaliana* sampled at day 13 compared with those at day 10 (MeOD/HEPES).

and analyzed at days 10, 13, 15, 19, and 23. The total amount of  $^{13}\text{C}$  from [ $^{13}\text{C}_6$ ]glucose in a plant became diluted over this period, suggesting that changes in the bondomer composition over the incubation periods were being observed efficiently. This notion was also supported by the incorporation profile of  $^{13}\text{CO}_2$ , which shows that the labeling ratio increased symmetrically with the decrease in the [ $^{13}\text{C}_6$ ]glucose labeling ratio. These data suggests that time-dependent changes in the bondomer composition can be observed in  $^1\text{H}$ – $^{13}\text{C}$  HSQC spectra under this incubation condition. Then we performed detailed analyses of the  $^{12}\text{CO}_2$  dilution profile, i.e., time-dependent cleavage of  $^{13}\text{C}$ – $^{13}\text{C}$  connectivities, for each metabolite using bondomer analyses in  $^1\text{H}$ – $^{13}\text{C}$  HSQC experiments.

### 2.2.2. Following metabolic dynamics in *A. thaliana*

Finally, we present examples of the time-dependent changes in the  $^{13}\text{C}$ – $^{13}\text{C}$  coupling pattern of [ $^{13}\text{C}_6$ ]glucose-labeled amino acids in *A. thaliana* with the assimilation of  $^{12}\text{CO}_2$ . Although the metabolites labeled with [ $^{13}\text{C}_6$ ]glucose in the plant samples had already been diluted by  $^{12}\text{CO}_2$  at day 10, the labeling ratio was sufficient for detect-

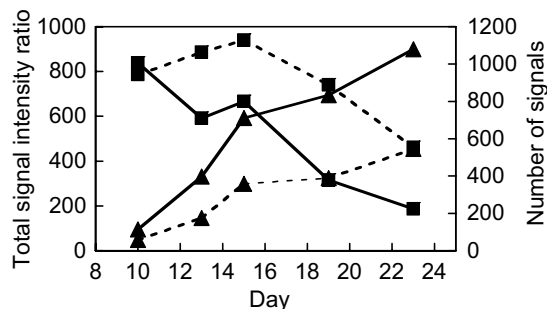


Fig. 4. Time course of [ $^{13}\text{C}_6$ ]glucose and  $^{13}\text{CO}_2$  incorporation into *A. thaliana*. The total signal intensities and numbers of signals observed in the  $^1\text{H}$ – $^{13}\text{C}$  HSQC spectra (MeOD/HEPES) were plotted against the incubation period (10, 13, 15, 19 and 23 days). The dotted line indicates the total HSQC signal intensity, and the solid line shows the number of signals. Filled rectangles are derived from [ $^{13}\text{C}_6$ ]glucose-labeled plants, and filled triangles are for  $^{13}\text{CO}_2$ -labeled plants.

ing fully labeled bondomers and observing  $^{13}\text{C}$ – $^{13}\text{C}$  bond cleavage. Furthermore, this incomplete labeling may help to detect additional introduced  $^{13}\text{C}$ – $^{13}\text{C}$  bond connectivities. Fig. 5 illustrates the  $^{13}\text{C}$ – $^{13}\text{C}$  coupling pattern at C2 of the amino acids in a crude MeOD/HEPES extract of [ $^{13}\text{C}_6$ ]glucose-labeled *A. thaliana*, sampled at days 13 and 23, and the  $^{13}\text{C}$ – $^{13}\text{C}$  connectivities deducible from the C2 coupling pattern. The  $^1J_{\text{CC}}$  values and deducible bondomer compositions are listed in Table 1. All of the  $^{13}\text{C}$ – $^{13}\text{C}$  connectivities observed in alanine, serine, and glycine at day 13 were cleaved completely by day 23. Each  $^1\text{H}$ – $^{13}\text{C}$  HSQC spectrum showed only the singlet signal, indicating that  $^{12}\text{C}$  from atmospheric  $\text{CO}_2$  was distributed uniformly into all of the carbons of these amino acids at this sampling point. This was supported by the  $^1\text{H}$ – $^{13}\text{C}$  HSQC signals of C3 of serine and alanine, which showed only clear singlet peaks (data not shown). Conversely, in the case of asparagine, a change in the  $^{13}\text{C}$ – $^{13}\text{C}$  bond position was observed. Instead of the doublet signal at 41.4 Hz that indicates C2–C3  $^{13}\text{C}$ – $^{13}\text{C}$  bond connectivity at day 13, a doublet peak at 48.3 Hz indicating C1–C2  $^{13}\text{C}$ – $^{13}\text{C}$  bond connectivity was observed at day 23. Therefore, although the  $^{13}\text{C}$  labeling of metabolites was uniformly diluted by atmospheric  $^{12}\text{CO}_2$ , the bias in the time-dependent contribution of  $\text{CO}_2$  assimilation via each biosynthetic pathway can be

observed using our strategy. The amount of deduced bondomers are represented by sum of the intensities of each signal of a multiplet (Table 1). As seen with asparagine, the  $^1J_{\text{CC}}$  value of C1–C2 of serine is extremely close to that of C2–C3, such that any overlapped singlet peak (s) cannot be distinguished in MeOD/HEPES. In HFA/HEPES, the difference between the  $^1J_{\text{CC}}$  values of C1–C2 and C2–C3 of serine is also sufficient to distinguish the singlet peak at C2 (supplementary section). It was confirmed by using HFA/HEPES that no singlet peak was observed at the C2 of serine at day 13. Concerning asparagine, the intensity of the singlet peak at day 23 was estimated based on the relative intensities of each signal of the *dd* observed at day 13 (1:2:1). As described above, we confirmed by changing solvent that no singlet peak was overlapped at C2 signal of asparagine at day 13. The ratio of the total intensities of all the bondomers of alanine and asparagine at day 23 to those at day 13 were 0.42 and 0.78, respectively. Compared to these amino acids, remarkable decreases were observed in the ratio of the intensities of the singlet signals of glycine (0.005) and serine (0.16) at day 23 to the total intensities of all the bondomers at day 13. Ideally, integrated information on all detectable metabolites will be obtained in the same way, and metabolic bias similar to that observed for amino acids should provide information on the biosyn-

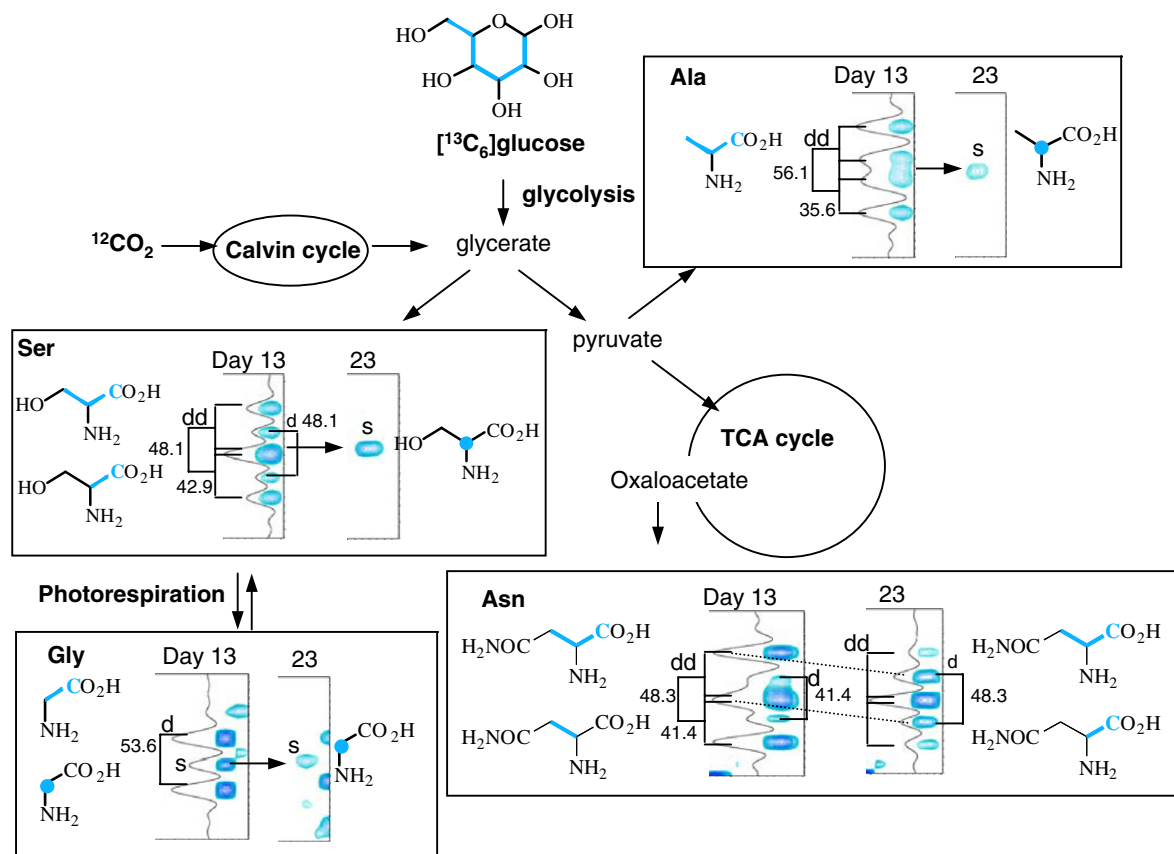
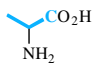
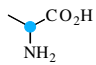
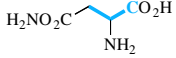
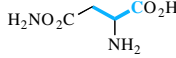
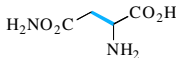
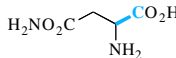
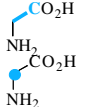
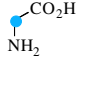
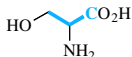
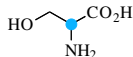
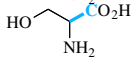


Fig. 5.  $^{13}\text{C}$ – $^{13}\text{C}$  coupling pattern at C2 of amino acids in [ $^{13}\text{C}_6$ ]glucose-labeled *A. thaliana* sampled at days 13 and 23 (MeOD/HEPES). Deducible  $^{13}\text{C}$ – $^{13}\text{C}$  bond connectivities from the C2 coupling pattern are indicated by blue lines.  $^1J_{\text{CC}}$  values are shown alongside in Hz. Ala,  $^1J_{\text{C1–C2}} = 56.1$  Hz,  $^1J_{\text{C2–C3}} = 35.6$  Hz; Asn,  $^1J_{\text{C1–C2}} = 48.3$  Hz,  $^1J_{\text{C2–C3}} = 41.4$  Hz; Gly,  $^1J_{\text{C1–C2}} = 53.6$  Hz; Ser,  $^1J_{\text{C1–C2}} = 48.1$  Hz,  $^1J_{\text{C2–C3}} = 42.9$  Hz. Details of all the measured coupling constants and the amount of each bondomer are listed in Table 1.

Table 1  
 $^{13}\text{C}$ – $^{13}\text{C}$  coupling pattern at C2 of amino acids and deducible  $^{13}\text{C}$ – $^{13}\text{C}$  connectivities in [ $^{13}\text{C}_6$ ]glucose-labeled *A. thaliana* sampled at days 13 and 23 (MeOD/HEPES)

Carbons	Day 13		Day 23	
	Observed multiplets	Relative intensity <sup>a</sup>	Observed multiplets	Relative intensity <sup>a</sup>
Ala C2	dd, $^1J_{\text{CC}} = 56.1, 35.6 \text{ Hz}^b$ C1–C2–C3 connectivity	 5.67	<i>s</i> No $^{13}\text{C}$ – $^{13}\text{C}$ connectivity at C2	 2.38
Asn C2	dd, $^1J_{\text{CC}} = 48.3, 41.4 \text{ Hz}$	 17.89	dd, $^1J_{\text{CC}} = 48.3, 41.4 \text{ Hz}$	 4.74 <sup>c</sup>
	C1–C2–C3 connectivity		C1–C2–C3 connectivity	
	<i>d</i> , $^1J_{\text{C2-C3}} = 41.4 \text{ Hz}$	 3.37	<i>d</i> , $^1J_{\text{C1-C2}} = 48.3 \text{ Hz}$	 1.3
Gly C2	<i>s</i> No $^{13}\text{C}$ – $^{13}\text{C}$ connectivity at C2	 5.69	<i>s</i> No $^{13}\text{C}$ – $^{13}\text{C}$ connectivity at C2	 0.17
	<i>d</i> , $^1J_{\text{CC}} = 53.6 \text{ Hz}$			
	C1–C2 connectivity			
Ser C2	dd, $^1J_{\text{CC}} = 48.1, 42.9 \text{ Hz}^b$	 7.18	<i>s</i> No $^{13}\text{C}$ – $^{13}\text{C}$ connectivity at C2	 1.58
	C1–C2–C3 connectivity			
	<i>d</i> , $^1J_{\text{C1-C2}} = 48.1 \text{ Hz}$	 2.96		
	C1–C2 connectivity			

<sup>a</sup> Sum of the intensities of each signal of a multiplet.

<sup>b</sup> No singlet peak was observed in HFA/HEPES.

<sup>c</sup> Estimated from the ratio of the intensities of each signal of the *dd* observed at day 13.

thetic relationships among metabolites at atomic level, and correlations among metabolic pathways.

### 3. Concluding remarks

We demonstrated the advantages of using a combination of different extraction solvents and pulse sequences for NMR-based fluxomics at the atomic level. One advantage of the measurement using different solvents is that it separates overlapped signals via chemical shift changes. Here, we focused on the separation of overlapped multiplets by changing the  $^1J_{\text{CC}}$  values to distinguish the bondomers. The  $^1J_{\text{CC}}$  values change in different solvents, making it possible to extract clear information about  $^{13}\text{C}$ – $^{13}\text{C}$  connectivities, which is necessary for the detailed elucidation of dynamic metabolic networks at the atomic level. The advantages of the combination of the  $^1\text{H}$ – $^{13}\text{C}$  HSQC experiment and other heteronuclear NMR techniques are exemplified by  $\text{C}\alpha$ -coupled and  $\text{C}\alpha$ -decoupled (normal) HCACO experiments to detect  $^{13}\text{C}$ – $^{13}\text{C}$  connectivities from the carbonyl carbon, which is an important functional group in biological systems but is invisible in  $^1\text{H}$ – $^{13}\text{C}$  HSQC spectra. The CO (C1)– $\text{C}\alpha$  (C2) connectivities in [ $^{13}\text{C}_6$ ]glucose-labeled *A. thaliana* can be monitored during incubation by the application of  $\text{C}\alpha$ -decoupled experiments. Finally, an example of the application of these methods, in combina-

tion with uniform stable isotope labeling, to metabolic network analysis was demonstrated. The bias in the time-dependent contribution of  $^{12}\text{CO}_2$  assimilation to the biosynthesis of each amino acid was observed in [ $^{13}\text{C}_6$ ]glucose-labeled *A. thaliana*.

We emphasize the importance of further methodological improvement of this measurement technology. A method for measuring a greater number of metabolic dynamics, which might be present in crude extracts as in this study, should enable the construction of a metabolic model that is more accurate than those obtained from a limited number of measured compounds. Therefore, we propose that future research should focus on further developments and applications of our strategy and should examine the changes in metabolic networks brought about by stress responses or gene disruption.

### 4. Experimental section

#### 4.1. General procedures and materials

##### 4.1.1. Chemicals

[ $^{13}\text{C}_6$ ]glucose (>98%  $^{13}\text{C}$ ) was purchased from Spectra Stable Isotopes. HFA · 3D<sub>2</sub>O and CD<sub>3</sub>OD (99.8% D) and HEPES-*d*<sub>18</sub> (98% D) were purchased from Cambridge Isotope Laboratories.

Deuterium oxide (99% D) were purchased from Aldrich. The gas mixture of 21% O<sub>2</sub>, 79% N<sub>2</sub>, and the desired <sup>13</sup>CO<sub>2</sub> concentration (345–350 ppm by volume) was purchased from Takachiho Chemical Industrial Co., Ltd.

#### 4.1.2. Plant materials and growth conditions

*Arabidopsis thaliana* ecotype Col was germinated and grown on Murashige and Skoog agar (pH 5.7) (Murashige and Skoog, 1962) at 22 °C under a 14-h light/10-h dark cycle at a light intensity of 90 μmol/m<sup>2</sup>s for 23 days, at which time flowering had not commenced. Thirty-two seed were placed on each Petri dish containing 30 ml of medium. For labeling with glucose, the medium was supplemented with [<sup>13</sup>C<sub>6</sub>]glucose (1%) and plates were allowed to stand in contact with ambient <sup>12</sup>CO<sub>2</sub>. For labeling in the presence of <sup>13</sup>CO<sub>2</sub> incorporation, the medium was supplemented with [<sup>12</sup>C<sub>6</sub>]glucose (1%) and incubated for 10 days under the same conditions as for [<sup>13</sup>C<sub>6</sub>]glucose labeling. The <sup>12</sup>C-glucose plates were then transferred into an airtight polycarbonate box filled with a gas mixture of 21% O<sub>2</sub>, 79% N<sub>2</sub>, and the desired <sup>13</sup>CO<sub>2</sub> concentration at 345–350 ppm by volume (Kikuchi and Hirayama, 2007). The rosettes were harvested after 7 h of light at days 10, 13, 15, 19, and 23.

#### 4.1.3. Preparation of NMR samples

The method for preparing NMR samples from plant samples was described previously and modified slightly (Kikuchi and Hirayama, 2007). Briefly, the lyophilized seedlings (3–10 plants) were ground to powder. This powder (3 mg) was suspended in 500 μl of MeOD/HEPES (10 mM, pH 7.0) or HFA/HEPES (40 mM, pH 7.0). The mixture was heated at 50 °C for 5 min, and centrifuged at 10,000g for 5 min. The supernatant was directly used for solution NMR experiments. MeOD/HEPES solution was composed of MeOD (47.5 ml), 1 M HEPES-*d*<sub>18</sub> solution (0.5 ml, pH 7.0) and D<sub>2</sub>O (2.0 ml). HFA/HEPES was solution composed of HFA · 3D<sub>2</sub>O (9 ml), 1 M HEPES-*d*<sub>18</sub> solution (0.4 ml, pH 7.0) and D<sub>2</sub>O (0.6 ml). Sodium 2,2-dimethyl-2-silapentane-5-sulfonate (DSS) was included in both of the solvents (0.5 mM in MeOD/HEPES and 1.0 mM in HFA/HEPES) as an internal standard.

#### 4.1.4. Solution NMR measurements

Sample solutions were transferred into 5-mm φ NMR tubes. All NMR spectra were recorded on a Bruker Avance-700 spectrometer equipped with an inverse triple resonance CryoProbe with a Z-axis gradient for 5 mm sample diameters operating at 700.153 MHz <sup>1</sup>H frequency (176.061 MHz for <sup>13</sup>C frequency), and the temperature of the NMR samples was maintained at 298 K. The NMR spectra were processed using NMRPipe software (Delaglio et al., 1995).

#### 4.1.5. Two-dimensional <sup>1</sup>H–<sup>13</sup>C HSQC analysis

The 2D <sup>1</sup>H–<sup>13</sup>C HSQC spectra (Bodenhausen and Ruben, 1980) were measured using the method described

by Kikuchi and Hirayama (2006). A total of 700 complex f1 (<sup>13</sup>C) and 2048 complex f2 (<sup>1</sup>H) points were recorded with eight scans per f1 increment, resulting in total recording times of about 6.5 h. The spectral window and offset frequency in the f1 dimension were 7042.593 Hz (40 ppm) and 11971.59 Hz (68 ppm), respectively. The spectral window in the f2 dimension was 11160.7 Hz (16 ppm). The offset frequency in the f2 dimension were 2333.70 Hz (3.3 ppm) for MeOD/HEPES extract or 3333.95 Hz (4.8 ppm) for HFA/HEPES extract. The chemical shifts were referenced to TMS group of internal DSS. To quantify the signal intensities, a Lorentzian-to-Gaussian window with a Lorentzian line width of 10 Hz and a Gaussian line width of 15 Hz was applied in both dimensions, before Fourier transformation. An automatic polynomial baseline correction was subsequently applied in the f1 dimension. The indirect dimension was zero-filled to 4096 points in the final data matrix.

#### 4.1.6. Two-dimensional HCACO analysis

The Cα-decoupled (normal) HCACO spectra (Kay et al., 1990b; Grzesiek and Bax, 1993) were recorded for a total of 128 complex f1 (<sup>13</sup>CO), 1 complex f2 (<sup>13</sup>Cα) and 1024 complex f3 (<sup>1</sup>H) points with 128 scans per f1 increment, resulting in total recording times of about 5 h. The repetition time was set to 1.5 s and delay times of 1/(4J<sub>H–Cα</sub>) and 1/(4J<sub>Cα–CO</sub>) were optimized at 2.1 ms and 4.5 ms, respectively. The spectral window and offset frequency in the f1 dimension were 1760.6 Hz (10 ppm) and 30457.1 Hz (173 ppm), respectively. The spectral window and offset frequency in the f2 dimension were 3169.1 Hz (18 ppm) and 10211.1 Hz (58 ppm), respectively. The spectral window and offset frequency in the f3 dimension were 4201.7 Hz (6.0 ppm) and 2800.6 Hz (4.0 ppm), respectively. The Cα-coupled HCACO experiments were performed by eliminating Cα 180° degree shaped pulse applied at the midpoint of CO evolution. The Cα-coupled HCACO spectra were recorded for a total of 64 complex f1 (<sup>13</sup>CO), 1 complex f2 (<sup>13</sup>Cα) and 1024 complex f3 (<sup>1</sup>H) points with 512 scans per f1 increment, resulting in total recording times of about 15 h. The spectral window and offset frequency are the same as described for the Cα-decoupled HCACO experiment. To quantify the signal intensities, a Lorentzian-to-Gaussian window with a Lorentzian line width of 5 Hz and a Gaussian line width of 10 Hz was applied in both dimensions, before Fourier transformation. An automatic polynomial baseline correction was subsequently applied in the f1 dimension. The indirect dimension was zero-filled to 256 points in the final data matrix.

#### Acknowledgements

The authors thank Eisuke Chikayama (RIKEN), Mami Okamoto (Yokohama City University), and Takashi Hirayama (RIKEN) for valuable discussions. This work



was supported in part by grants from the RIKEN President's Special Research Grant (No. A88-54366 to J.K.), CREST, the Japan Science and Technology Agency (J.K.), and the Ministry of Education, Culture, Sports, Science and Technology of Japan (No. 17710191 to J.K.).

## Appendix A. Supplementary data

Supplementary data associated with this article can be found, in the online version, at [doi:10.1016/j.phytochem.2007.04.011](https://doi.org/10.1016/j.phytochem.2007.04.011).

## References

- Birkemeyer, C., Luedemann, A., Wagner, C., Erban, A., Kopka, J., 2005. Metabolome analysis: the potential of *in vivo* labeling with stable isotopes for metabolite profiling. *Trends Biotechnol.* 23, 28–33.
- Bodenhausen, G., Ruben, D.J., 1980. Natural abundance nitrogen-15 NMR by enhanced heteronuclear spectroscopy. *Chem. Phys. Lett.* 69, 185–189.
- Buncel, E., Jones, J.R., 1991. Isotopic applications in NMR studies. In: *Isotopes in the Physical and Biomedical Sciences*, vol. 2. Elsevier, Amsterdam, Oxford, New York, Tokyo.
- de Graaf, A.A., Mahle, M., Möllney, M., Wiechert, W., Stahmann, P., Sahm, H., 2000. Determination of full  $^{13}\text{C}$  isotopomer distributions for metabolic flux analysis using heteronuclear spin echo difference NMR spectroscopy. *J. Biotech.* 77, 25–35.
- Delaglio, F., Grzesiek, S., Vuister, G.W., Zhu, G., Pfeifer, J., Bax, A., 1995. A multidimensional spectral processing system based on UNIX pipes. *J. Biomol. NMR* 6, 277–293.
- Glawischnig, E., Gierl, A., Tomas, A., Bacher, A., Eisenreich, W., 2001. Retrobiosynthetic nuclear magnetic resonance analysis of amino acid biosynthesis and intermediary metabolism. Metabolic flux in developing maize kernels. *Plant Physiol.* 125, 1178–1186.
- Govil, G., 2004. Metabonomics: a new frontier of nuclear magnetic resonance (NMR). *Natl. Acad. Sci. Lett.* 27, 289–299.
- Grzesiek, S., Bax, A., 1993. An origin and removable of artifacts in 3D HCACO spectra of proteins uniformly enriched with  $^{13}\text{C}$ . *J. Magn. Reson. Ser. B* 102, 103–106.
- Hall, R.D., 2005. Plant metabolomics: from holistic hope, to hype, to hot topic. *New Phytologist* 169, 453–458.
- Hansen, P.E., 1978. Long-range  $^{13}\text{C}$ – $^{13}\text{C}$  coupling constants. A review. *Org. Magn. Reson.* 11, 215–233.
- Horiuchi, T., Takahashi, M., Kikuchi, J., Yokoyama, S., Maeda, H., 2005. Effect of dielectric properties of solvents on the quality factor for a beyond 900 MHz cryogenic cooled probe model. *J. Magn. Reson.* 174, 32–42.
- Jones, J.G., Solomon, M.A., Cole, S.M., Sherry, D., Malloy, C.R., 2001. An integrated  $^2\text{H}$  and  $^{13}\text{C}$  NMR study of gluconeogenesis and TCA cycle flux in humans. *Am. J. Physiol. Endocrinol. Metab.* 281, E848–E856.
- Kamińska-Trela, K., 1995. One-bond  $^{13}\text{C}$ – $^{13}\text{C}$  spin coupling constants. *Annu. Rep. NMR Spectrosc.* 30, 131–230.
- Kay, L.E., Ikura, M., Bax, A., 1990a. Proton–proton couplings via carbon–carbon couplings. A three-dimensional NMR approach for assignments of aliphatic resonances in proteins labeled with carbon-13. *J. Am. Chem. Soc.* 112, 888–889.
- Kay, L.E., Ikura, M., Tschudin, R., Bax, A., 1990b. Three-dimensional triple-resonance NMR spectroscopy of isotopically enriched proteins. *J. Magn. Reson.* 89, 496–514.
- Kikuchi, J., Shinozaki, K., Hirayama, T., 2004. Stable isotope labeling of *Arabidopsis thaliana* for a hetero-nuclear NMR-based metabolomics. *Plant Cell Physiol.* 45, 1099–1104.
- Kikuchi, J., Hirayama, T., 2006. Hetero-nuclear NMR-based metabolomics. In: Saito, K., Dixon, R.A., Willmitzer, L. (Eds.), *Biotechnology in Agriculture and Forestry, Plant Metabolomics*, vol. 57. Springer-Verlag, Berlin Heidelberg, pp. 93–101.
- Kikuchi, J., Hirayama, T., 2007. Practical aspects of stable isotope labeling of higher plants for hetero-nuclear NMR-based metabolomics. *Method Mol. Biol.* 358, 273–286.
- Korir, A.K., Almeida, V.K., Malkin, D.S., Larvie, C.K., 2005. Separation and analysis of nanomole quantities of heparin oligosaccharides using on-line capillary isotachopheresis coupled with NMR detection. *Anal. Chem.* 77, 5998–6003.
- Kromer, J.O., Sorgenfrei, O., Klopprogge, K., Heinze, E., Wittmann, C., 2004. In-depth profiling of lysine-producing *Corynebacterium glutamicum* by combined analysis of the transcriptome, metabolome, and fluxome. *J. Bacteriol.* 186, 1769–1784.
- Krivin, L.B., Kalabin, G.A., 1988. Directly bonded  $^{13}\text{C}$ – $^{13}\text{C}$  spin–spin coupling constants in structural studies. *Russ. Chem. Rev.* 57, 1–17.
- Kruger, N.J., Ratcliffe, R.G., Roscher, A., 2003. Quantitative approaches for analysing fluxes through plant metabolic networks using NMR and stable isotope labeling. *Phytochem. Rev.* 2, 17–30.
- Lee, S.-Y., Lee, D.-Y., Kim, T.-Y., 2005. Systems biotechnology for strain improvement. *Trends Biotechnol.* 23, 349–358.
- Li, Y., Webb, A.G., Saha, S., Brey, W.W., Zachariah, C., Edison, A.S., 2006. Comparison of the performance of round and rectangular wire in small solenoids for high-field NMR. *Magn. Reson. Chem.* 44, 255–262.
- London, R.E., 1988.  $^{13}\text{C}$  labeling in studies of metabolic regulation. *Prog. NMR Spectrosc.* 20, 337–383.
- Maciel, G.E., 1974.  $^{13}\text{C}$ – $^{13}\text{C}$  coupling constants. In: *NMR Spectroscopy of Nuclei Other Than Protons*. Wiley-Interscience, New York, pp. 187–218.
- Mooney, E.F., Winson, P.H., 1969. Carbon-13 nuclear magnetic resonance spectroscopy: carbon-13 chemical shifts and coupling constants. *Annu. Rev. NMR Spectrosc.* 2, 153–218.
- Murashige, T., Skoog, F.A., 1962. A revised medium for rapid growth and bioassays with tobacco tissue culture. *Physiol. Plant* 15, 473–497.
- Nielsen, J., 2003. It is all about metabolic fluxes. *J. Bacteriol.* 185, 7031–7035.
- Nielsen, J., Oliver, S., 2005. The next wave in metabolome analysis. *Trend. Biotechnol.* 23, 544–546.
- Pan, Z., Raftery, D., 2007. Comparing and combining NMR spectroscopy and mass spectrometry in metabolomics. *Anal. Bioanal. Chem.* 387, 525–527.
- Petersen, S., de Graaf, A.A., Eggeling, L., Möllney, M., Wiechert, W., Sahm, H., 2000. *In vivo* quantification of parallel and bidirectional fluxes in the anaplerosis of *Corynebacterium glutamicum*. *J. Biol. Chem.* 275, 35932–35941.
- Ratcliffe, R.G., Roscher, A., Shachar-Hill, Y., 2001. Plant NMR spectroscopy. *Prog. Nucl. Magn. Reson. Spectrosc.* 39, 267–300.
- Ratcliffe, R.G., Shachar-Hill, Y., 2001. Probing plant metabolism with NMR. *Annu. Rev. Plant Physiol. Plant Mol. Biol.* 52, 499–526.
- Ratcliffe, R.G., Shachar-Hill, Y., 2005. Revealing metabolic phenotypes in plants: inputs from NMR analysis. *Biol. Rev.* 80, 27–43.
- Ratcliffe, R.G., Shachar-Hill, Y., 2006. Measuring multiple fluxes through plant metabolic networks. *Plant J.* 45, 490–511.
- Roberts, J.K.M., 2000. NMR adventures in the metabolic labyrinth within plants. *Trends Plant Sci.* 5, 30–34.
- Roscher, A., Kruger, N.J., Ratcliffe, G., 2000. Strategies for metabolic flux analysis in plants using labeling. *J. Biotechnol.* 77, 81–102.
- Sanford, K., Soucaille, P., Whited, G., Chotani, G., 2001. Genomics to fluxomics and physiomics—pathway engineering. *Curr. Opin. Microbiol.* 5, 318–322.
- Sauer, U., Lasko, D.R., Fiaux, J., Hochuli, M., Glaser, R., Szyperski, T., Wuthrich, K., Bailey, J.E., 1999. Metabolic flux ratio analysis of genetic and environmental modulations of *Escherichia coli* central carbon metabolism. *J. Bacteriol.* 181, 6679–6688.
- Sauer, U., 2004. High-throughput phenomics: experimental methods for mapping fluxomes. *Curr. Opin. Biotechnol.* 15, 58–63.

- Sauer, U., 2006. Metabolic networks in motion:  $^{13}\text{C}$ -based flux analysis. *Mol. Syst. Biol.* 62, 1–10.
- Schmidt, K., Nielsen, J., Villadsen, J., 1999. Quantitative analysis of metabolic fluxes in *Escherichia coli*, using two-dimensional NMR spectroscopy and complete isotopomer models. *J. Biotechnol.* 71, 175–190.
- Siram, G., Fulton, D.B., Iyer, V.V., Peterson, J.M., Zhou, R., Westgate, M.E., Spalding, M.H., Shanks, J.V., 2004. Quantification of compartmented metabolic fluxes in developing soybean embryos by employing biosynthetically directed fractional  $^{13}\text{C}$  labeling, Two-dimensional [ $^{13}\text{C}$ ,  $^1\text{H}$ ] Nuclear magnetic resonance, and comprehensive isotopomer blanching. *Plant Physiol.* 136, 3043–3057.
- Szyperki, T., 1995. Biosynthetically directed fractional  $^{13}\text{C}$ -labeling of proteinogenic amino acids. An efficient analytical tool to investigate intermediary metabolism. *Eur. J. Biochem.* 232, 433–448.
- Szyperki, T., Bailey, J.E., Wüthrich, K., 1996. Detecting and dissecting metabolic fluxes using biosynthetic fractional  $^{13}\text{C}$  labeling and two-dimensional NMR spectroscopy. *Trends Biotechnol.* 14, 453–459.
- Tang, Y.J., Hwang, J.S., Wemmer, D.E., Keasling, J.D., 2007. The *Shewanella oneidensis* MR-1 fluxome under various oxygen conditions. *Appl. Env. Microbiol.*, in press.
- Tian, C.J., Chikayama, E., Tsuboi, Y., Kuromori, T., Shinozaki, K., Kikuchi, J., Hirayama, T., 2007. Top-down phenomics of *Arabidopsis thaliana* –One and two-dimensional NMR metabolic profiling and transcriptome analysis of albino mutants. *J. Biol. Chem.*, in press.
- van Winden, W.A., Heijnen, J.J., Verheijen, P.J.T., 2002. Cumulative bondomers: a new concept in flux analysis from 2D [ $^{13}\text{C}$ ,  $^1\text{H}$ ] COSY NMR data. *Biotechnol. Bioeng.* 80, 731–745.
- Wang, Q.-Z., Wu, C.-Y., Chen, T., Chen, X., Zhao, X.-M., 2006. Integrating metabolomics into systems biology framework to exploit metabolic complexity: strategies and applications in microorganisms. *Appl. Microbiol. Biotech.* 70, 151–161.
- Wendish, V.F., Bott, M., Kalinowski, J., Oliges, M., Wiechert, W., 2006. Emerging *Corynebacterium glutamicum* systems biology. *J. Biotechnol.* 124, 74–92.
- Yang, C., Hua, Q., Shimizu, K., 2002. Quantitative analysis of intracellular metabolic fluxes using GC-MS and two-dimensional NMR spectroscopy. *J. Biosci. Bioeng.* 93, 78–87.
- Zamboni, N., Sauer, U., 2005. Fluxome profiling in microbes. In: *Metabolome analysis: Strategies for systems biology*. Springer, New York, pp. 307–322.